ORCID Details: 1 https://orcid.org/0009-0001-2810-5336

DECLARATION

This manuscript is being submitted for publication in the Journal of Climate (AMS). Please note that it is yet to undergo peer review and is yet to be formally accepted for publication. Subsequent versions of this manuscript may have slightly different content. If accepted, the final version of this manuscript will be available via the 'Peer-reviewed Publication DOI' link on the right-hand side of this webpage. Please feel free to contact any of the authors; we welcome feedback.

Title of the Article

A Mechanism Criterion Replaces Coupling Magnitude for Rainfall Inhibitory Skill Across Three Indo-Pacific Forcing Modes

Author
Mr Pochender Shenigarapu
Doctoral Research Scholar
Jawaharlal Nehru Technological University Anantapur
Anantapuramu – 515002
INDIA
Pochender.ce.scholar@gprec.ac.in
https://orcid.org/0009-0001-2810-5336

Co Author
Dr. Prof. Sanjeeva Rayudu Ekkaluri
Asst. Professor
G Pulla Reddy Engineering College, Kurnool – 518007
INDIA
Sanjeeva.ce@gprec.ac.in

Corresponding Author
Mr Pochender Shenigarapu
Pochender.ce.scholar@gprec.ac.in

Submitted to: npj Climate and Atmospheric Science
Intraseasonal analysis period: 1 January 2001 – 31 December 2020 (MJO arm)
Interannual analysis period: 1 January 1995 – 31 December 2024 (ENSO/IOD arm)

A Mechanism Criterion Replaces Coupling Magnitude for Rainfall Inhibitory Skill Across Three Indo-Pacific Forcing Modes

Abstract

CPAdry — the Conditional Precipitation Anomaly, dry phase — detects rainfall inhibitory mechanism failure across three forcing modes: the MJO (intraseasonal), ENSO, and IOD (interannual). Twenty assessments at eighteen Indo-Pacific sites using two-track methodology establish the governing principle: CPAdry returns meaningful skill only where the forcing mode imposes locally active inhibition, not where it acts through remote teleconnection — and this holds regardless of coupling magnitude. At MJO direct-passage sites, diagnostic skill is strong and rising with lead time; at all passive sites it collapses to chance, with the highest-coupled passive site — Colombo — serving as the central falsifying case. Across the ENSO/IOD arm, four active-mechanism sites spanning warm-pool displacement, Walker relay, thermocline-tilt, and extratropical Rossby wave pathways confirm the same bifurcation with high to moderate skill. Three cross-timescale synthesis findings emerge. First, MJO phase state does not condition ENSO/IOD skill ($p = 0.94$): ENSO and IOD establish the suppressive umbrella; MJO contributions are absorbed by the accumulation window. Second, a three-layer conditional suppression structure at Colombo reveals that NegIOD alone produces −11.6% suppressive anomaly while NegIOD combined with active MJO produces −28.4% and twelve events — neither crosses the −25% threshold alone. Third, this conditional suppressibility is unique to Colombo across the entire non-active network. The coupling-magnitude proxy is replaced by a sign-discriminated suppressive anomaly criterion that correctly classifies all twenty assessments without skill computation.

Keywords: Subseasonal-to-Seasonal Prediction; Madden–Julian Oscillation; ENSO Teleconnections; Indian Ocean Dipole; Rainfall Inhibitory Mechanisms; Convective Regime; Diagnostic Skill; Compound Forcing; Indo-Pacific Rainfall; Phase-Conditional Climatology; East Africa Short Rains.

1. Introduction

Rainfall diagnostic frameworks across the Indo-Pacific have a characteristic failure mode (Madden and Julian, 1971, 1972, 1994; Zhang, 2005). They establish a statistical coupling between a large-scale climate-forcing mode and local rainfall, then treat that coupling as a license to deploy phase-conditioned predictive skill. The coupling is real. The skill, very often, is not. The gap between the two is structural: coupling magnitude, measured as the eta-squared (η^2) effect size from phase-stratified ANOVA, is symmetric with respect to the direction and mechanism of the coupling. It registers a +55% enhancement and a −55% suppression with equal statistical weight. It cannot distinguish a site where the forcing mode imposes locally active dynamic inhibition from a site where the same mode modulates rainfall through a remote moisture flux pathway. These are mechanistically distinct regimes. They produce identical coupling statistics and produce, respectively, significant diagnostic skill and zero skill. No η^2 threshold separates them.

The diagnostic vehicle introduced here is CPAdry — the Conditional Precipitation Anomaly, dry phase. It measures the departure of rolling suppressive-phase heavy-rain frequency from its phase-conditioned climatological expectation, standardised by day of year to remove seasonal structure. The physical premise is precise. Where a forcing mode imposes direct local inhibition, that inhibition fails in a coherent, detectable way. An override mechanism must actively compete with and defeat the inhibitory forcing (Mapes, 2000). That competition accumulates a prior signal across the rolling window. CPAdry

measures that accumulation. Where forcing operates remotely, no local inhibitory barrier exists. No override is required. No signal accumulates. The AUC returns to 0.50 — not as underperformance, but as the correct diagnostic verdict for a passive regime.

Two analytical arms, each calibrated to the physical timescale of its forcing mode, produce twenty assessments at eighteen unique Indo-Pacific sites. The seven-site MJO arm spans direct convective envelope passage, post-barrier attenuation, remote teleconnection, and null coupling across the 2001–2020 record. The thirteen-site ENSO/IOD arm spans warm-pool core suppression, Walker Circulation relay, western-pole IOD thermocline forcing, extratropical Rossby wave propagation, and four distinct boundary condition types across the 1995–2024 record. Colombo and Mombasa appear in both arms as cross-timescale anchors. That overlap is deliberate: it tests directly whether a site passive under one forcing mode remains passive under another, and whether joint forcing across timescales changes the diagnostic verdict.

Three synthesis findings emerge that neither arm alone can produce. First, MJO phase state does not condition ENSO/IOD CPAdry skill — ENSO and IOD establish the dominant suppressive umbrella, within which MJO contributions are absorbed by the ninety-day accumulation window without explicit stratification. Second, the Colombo paradox is resolved: NegIOD and active MJO together cross the inhibitory threshold that neither crosses alone, generating twelve conditional DPS events against zero from either forcing alone. Third, that conditional suppressibility is unique to Colombo across the full combined network. Each finding is visible only from within the joint architecture. None is accessible from within a single arm.

A note on self-referencing. The MJO arm results reported here replicate the analysis of Shenigarapu and Ekkaluri (2026), available on EarthArXiv.Preprint, (https://doi.org/12276) using identical data and confirmed methodology. Agreement is expected because the underlying physics is real. The ENSO/IOD arm constitutes original analysis not previously published. All results in both arms are computed within this study from the data and code described in Section 3.

Section 2 describes data and the eighteen-site network. Section 3 presents the two-track methodology. Section 4 reports MJO arm results. Section 5 reports ENSO/IOD arm results. Section 6 presents the three synthesis findings. Section 7 develops the hierarchical forcing framework. Section 8 concludes.

2. Data and Study Network

2.1 Precipitation Data

Daily precipitation at all eighteen sites comes from MERRA-2 (Gelaro et al., 2017; Reichle et al., 2017; Bosilovich et al., 2015) — specifically the PRECTOTCORR corrected total precipitation variable (mm day^{-1}), accessed via the NASA POWER portal (Stackhouse et al., 2018). The MJO arm draws on the 2001–2020 record; the ENSO/IOD arm on 1995–2024. Both records are complete with no missing values.

MERRA-2 PRECTOTCORR is a conservative lower bound on point-scale CPAdry skill at local-amplitude sites, a property confirmed by Bureau of Meteorology gauge validation at Darwin (Station -14015, 2001-2020) and qualified by gauge validation at Adelaide (Station 023034, 1995 – 2024) completed within this study. Whether MERRA-2 acts as a conservative floor or a modest ceiling depends on the spatial scale of the local inhibitory mechanism – a finding developed in full in Section 5.2 and discussed in Section 7.4.

2.2 Climate Indices

MJO phase and amplitude come from the Wheeler–Hendon Real-time Multivariate MJO index (Wheeler & Hendon, 2004), BoM archive. Active MJO days carry RMM amplitude ≥ 1.0. The archive runs to 2024-02-24; the remaining 2024 days receive amplitude zero and are excluded from all phase-conditional analysis. The ENSO phase is the Niño3.4 SST anomaly relative to the 1991–2020 WMO baseline (NOAA CPC, threshold ±0.5°C) (Trenberth, 1997). IOD phase is the Dipole Mode Index of Saji et al. (1999) from JAMSTEC, standard threshold ±0.4°C. At Dar es Salaam, where the standard threshold yields a marginal DPS sample, a sensitivity threshold of ±0.3°C is applied.

2.3 Eighteen-Site Network

The network is designed for structural contrast, not geographic coverage. Every site either confirms a mechanism prediction or falsifies one. Table 1 presents all eighteen sites with their classification and primary results.

Table 1 presents all eighteen sites. Colombo and Mombasa appear in both arms – a deliberate overlap that tests whether a site passive under one forcing mode remains passive under another and whether joint forcing across timescales changes the diagnostic verdict. It does, at Colombo alone.

Site	Coordinates	Season	Forcing	Classification	AUC t+10	η^2 (%)
Darwin	**12.45°S 130.84°E**	**Oct–Apr**	**MJO**	**Active-Direct (MJO)**	**0.758**	**7.5**
Dili	**8.56°S 125.58°E**	**Nov–Mar**	**MJO**	**Active-Direct (MJO)**	**0.744**	**6.7**
Makassar	5.15°S 119.43°E	Nov–Mar	MJO	Active-Attenuated (MJO)	0.557	4.0
Colombo*	6.93°N 79.86°E	Oct–Jan/Dec	MJO+IOD	Passive→Conditional	0.50 / —	11.2 / 4.1
Mombasa*	4.05°S 39.67°E	Oct–Dec	MJO+IOD	Passive / Type IV	0.52 / —	3.7 / 6.3
Port Moresby	9.45°S 147.18°E	Dec–Apr	MJO	Passive-Attenuated (MJO)	0.549	1.5
Niamey	13.51°N 2.10°E	Jun–Sep	MJO	Passive-Absent (MJO)	0.50	1.0
Nauru	**0.55°S 166.92°E**	**Nov–Apr**	**ENSO**	**Active-Core (ENSO)**	**0.861**	**12.4**
Bulawayo	20.02°S 28.63°E	Nov–Mar	ENSO	Active-Remote (ENSO)	0.684	0.93
Dar es Salaam	6.81°S 39.29°E	Oct–Jan	IOD	Active-West-Pole (IOD)	0.751	2.04
Adelaide	34.94°S 138.54°E	Jul–Oct	IOD	Active-Extratropical (IOD)	0.673	1.00
Funafuti	8.52°S 179.20°E	Nov–Apr	ENSO	Type II Sub-threshold	—	1.98
Puerto Ayora	0.74°S 90.32°W	Jan–May	ENSO	Type I Enhancement	—	1.40
Guayaquil	2.16°S 79.88°W	Jan–May	ENSO	Type I Enhancement	—	1.35
Padang	0.95°S 100.36°E	Oct–Feb	IOD	Type III Wet-site	—	0.41
Seychelles	4.69°S 55.47°E	Nov–Mar	IOD	Type II Sub-threshold	—	1.39
Malé	4.17°N 73.51°E	May–Oct	IOD	IOD-Node	—	0.06
Chennai	12.99°N 80.18°E	Oct–Dec	IOD	Type I Enhancement	—	0.44

Table 1. Eighteen-site network producing twenty analytical assessments. * Colombo and Mombasa appear in both arms. Blue rows: MJO arm (7 sites, 2001–2020). Green rows: active ENSO/IOD sites (4 sites, 1995–2024). Grey rows: non-active ENSO/IOD sites (9 sites). AUC shown at t+10 for active sites; η^2 shows primary forcing arm value.

3. Methodology: Two-Track CPAdry

CPAdry asks one diagnostic question at every site and in every arm: does a locally active inhibitory mechanism fail detectably? The question is invariant. The parameters that operationalise it differ between the MJO and ENSO/IOD arms because the forcing modes operate on fundamentally different physical timescales. A 60-day window spans one MJO propagation cycle — the minimum for stable phase-conditional accumulation. A 90-day window spans one IOD development phase — the minimum for capturing the slow-building suppressive trajectory that characterises interannual forcing. A single parameter set applied uniformly across subseasonal and interannual forcing would be methodologically incorrect. The two-track design is a scientific requirement, not an inconsistency. Table 2 records the full parameter specification and the physical justification for each choice.

Parameter	MJO Arm	ENSO/IOD Arm	Physical Justification
Rolling window	60 days (centred)	90 days (backward)	60 days spans one MJO cycle — minimum for stable phase-conditional statistics. 90 days spans one IOD development phase — captures the slow-developing suppressive trajectory.
Heavy-rain threshold	P75 (>= 75th percentile)	P90 (>= 90th percentile)	MJO suppressive events involve moderate-to-heavy rainfall departures. ENSO/IOD suppression is more complete; P90 targets genuinely anomalous events within a suppressed regime.
Persistence guard	3 days	10 days	3 days reflects MJO-regime convective moisture memory in the Maritime Continent monsoon. 10 days reflects longer synoptic moisture memory within ENSO/IOD boundary conditions.
Analysis period	2001–2020	1995–2024	MJO arm matches SE26 preprint (Shenigarapu & Ekkaluri, 2026). ENSO/IOD arm uses 30 years for stable stratified ANOVA across three ENSO states.
Min DPS threshold	75–100 events	30 events	MJO-arm P75 generates denser event pools. ENSO/IOD three-tier reporting (Full ≥ 30; Directional 15–29; Below threshold < 15) applies.
Suppressive phase criterion	−25% of wet-season active-MJO mean	−25% of all-phase wet-season mean	Identical physical criterion: phases with rainfall more than 25% below the relevant all-condition mean.

Table 2. Two-track CPAdry parameter specifications. Both tracks share RMM amplitude ≥ 1.0 for active-MJO classification and a ±15-day centred DOY window for threshold computation.

3.1 CPAdry Architecture

The CPAdry formula is shared across both arms, but its components are calibrated separately to each arm's physical timescale.

For the ENSO/IOD arm, let $f^{\text{obs}}(t)$ denote the observed heavy-rain frequency among strongly suppressive forcing-phase days within the ninety-day backward window ending at day t, where heavy rain is defined by exceedance of the site-specific seasonally varying P90 threshold:

$$f^{\text{obs}}(t) = \frac{1}{|W|} \sum_{\tau \in W} \mathbb{1}[P(\tau) \geq P_{90}(\text{DOY}(\tau))]$$

Let $f^{\text{clim}}(\varphi, m)$be the phase-month climatological expectation and $\sigma^{\text{clim}}(\varphi, m)$its cross-condition standard deviation. Then:

$$\text{CPAdry}(t) = \frac{f^{\text{obs}}(t) - f^{\text{clim}}(\varphi, m)}{\sigma^{\text{clim}}(\varphi, m)}$$

A positive value signals suppression failure — the suppressive phase is delivering heavy rain at a rate above its climatological norm. A negative value signals suppression holding.

The departure is signed. A positive value signals suppression failure — the suppressive phase is delivering heavy rain at a rate above its climatological norm. A negative value signals suppression holding.

For the MJO arm, the climatological expectation is computed per (phase, DOY) pair using a ±30-day centred window with 31-day uniform smoothing, and the departure is absolute rather than signed:

$$\text{CPAdry}(t) = \frac{|\, f^{\text{obs}}(t) - f^{\text{clim}}(\varphi, \text{DOY}(t)) \,|}{\sigma^{\text{clim}}(\varphi, \text{DOY}(t))}$$

The absolute departure is adopted because the signed form correlates with rolling rainfall at Darwin (Spearman $\rho = 0.672$), making it a rainfall proxy rather than a mechanism-conditional signal. Absolute departure eliminates this correlation ($\rho = -0.009$ at Darwin, $\rho = 0.022$at Dili).

It captures genuine phase-conditional anomaly regardless of the direction of the deviation. The ENSO/IOD arm uses signed departure because the directional suppression trajectory — accumulating below climatology as the IOD deepens — carries informational content that absolute departure would discard.

At both arms, CPAdry is standardised to day-of-year to remove residual seasonal structure before AUC evaluation. Independence from rolling rainfall is verified at every active site before the metric is used as a predictor. It is not assumed.

3.2 DPS Event Definition

A Dry-Phase Surprise (DPS) event is the prediction target. It is defined precisely to avoid tautology: the metric that predicts it — CPAdry — must be architecturally independent of the rainfall magnitude that defines it. The independence verification described above confirms this. CPAdry measures phase-conditional probability departure. A DPS event is heavy rainfall on a suppressive day. The two draw on different information sources by construction.

In the ENSO/IOD arm, day t qualifies as a DPS event if three conditions hold simultaneously. The forcing phase must be strongly suppressive — any phase whose wet-season mean rainfall falls more than 25% below the all-phase grand mean. Daily rainfall must meet or exceed the site-specific P90 threshold, computed from a ±15-day centred DOY window to preserve seasonal structure. And no heavy-rain day may have occurred in the preceding ten calendar days — the persistence guard.

Formally, day $t$qualifies as a DPS event in the ENSO/IOD arm if and only if:

$$A_{\phi(t)} \leq -25\% \;\cap\; P(t) \geq P_{90}(\text{DOY}(t)) \;\cap\; \nexists\, \tau \in (t-10, t) : P(\tau) \geq P_{90}(\text{DOY}(\tau)) \wedge \phi(\tau) \notin \Phi_s$$

where $\phi(t)$is the forcing phase on day t, $\Phi_s$is the set of strongly suppressive phases satisfying $A_\phi \leq -25\%$, and the third condition is the persistence guard excluding non-suppressive heavy-rain days within the preceding ten calendar days.

This guard matters because ENSO/IOD boundary conditions sustain multi-day synoptic moisture anomalies (DeMott et al., 2015). Without it, a storm system beginning during a non-suppressive phase and persisting into a suppressive phase would register as a DPS event. It is not one. It is storm-system memory. The guard targets only non-suppressive heavy-rain days: rainfall that occurs during the suppressive phase itself does not trigger the guard, because that is the event the framework seeks to understand.

In the MJO arm, two conditions apply: the MJO phase must be strongly suppressive with RMM amplitude ≥ 1.0 (Wheeler & Hendon, 2004; Straub, 2013), and daily rainfall must meet or exceed the site-specific P75 threshold. No persistence guard is applied. The intraseasonal timescale of the MJO is short enough that storm-system memory does not contaminate the event pool in the way it does under interannual boundary forcing. Removing the guard recovers the verified DPS counts that underpin the MJO preprint results, and the absence of the guard is explicitly documented in the reproducibility record.

A minimum of thirty DPS events is required for AUC evaluation at any site. Where the sample falls between fifteen and twenty-nine, results are reported directionally with wide confidence intervals. Below fifteen, no AUC is computed.

3.3 Skill Evaluation

Skill is evaluated as AUC in the Mann-Whitney sense (Hanley & McNeil, 1982; Mason & Graham, 2002; Pepe, 2003; Jolliffe & Stephenson, 2003; Wilks, 2019; Suematsu et al., 2024):

$$AUC=P(CPAdry_{DPS}>CPAdry_{non\text{-}DPS})$$

where the probability is estimated over all pairs of randomly selected DPS and non-DPS days at lead k. AUC = 0.50 indicates no discrimination; AUC = 1.00 indicates perfect discrimination.

Statistical significance is assessed using the Hanley-McNeil standard error under the one-tailed null AUC ≤ 0.50. This is the correct test for a directional prediction: the metric is designed to be high before DPS events and low otherwise, not merely different.

Three baselines accompany CPAdry at every lead. Same-day raw rainfall Rain(t) tests whether CPAdry is simply measuring concurrent rainfall magnitude rather than a phase-conditional prior signal. Rolling rainfall mean R_W(t) — W = 60 days for the MJO arm, W = 90 days for the ENSO/IOD arm, DOY-standardised identically to CPAdry — tests whether CPAdry carries information beyond the broad seasonal regime. Five-day rolling standard deviation RollSD5d(t) tests whether CPAdry is exploiting recent weather-scale variability. The baseline comparison framework follows Murphy (1988). CPAdry advantage is defined as AUC(CPAdry) − AUC(R_W). A positive advantage that is sustained across the primary evaluation window — not present at one lead and absent at another — constitutes evidence of genuine phase-conditional diagnostic content that the regime baseline cannot reproduce.

The comparison against Rain(t) is particularly important. If AUC(CPAdry) ≈ AUC(Rain) at short leads, the metric is a rainfall proxy. The two diverge sharply at active-mechanism sites: Rain(t) AUC at Darwin falls from 0.766 at t+0 to 0.458 at t+10, precisely the window over which CPAdry rises. They draw on different information. That divergence is the diagnostic signature of a regime-scale prior signal.

3.4 MJO Modulation Test

The modulation test is pre-specified in full before any ENSO/IOD computation runs. Its design follows directly from the hierarchical hypothesis: if ENSO and IOD establish the dominant suppressive umbrella, MJO phase state should not systematically alter CPAdry skill within that umbrella. The test asks this question directly.

At each of the four active ENSO/IOD sites, suppressive-phase wet-season days are partitioned into three subsets: MJO-inactive (RMM amplitude < 1.0), MJO-constructive (active MJO in a phase that reinforces the interannual suppression at that site), and MJO-destructive (active MJO in a phase that competes with the interannual suppression). MJO phase assignments to constructive and destructive categories are locked from the MJO arm's confirmed suppressive phase geography before any ENSO/IOD AUC computation begins. They are not adjusted post-hoc.

The primary comparison tests the null hypothesis:

$$H_0: \mathrm{AUC}_{\mathrm{constructive}} = \mathrm{AUC}_{\mathrm{inactive}} \text{ at lead } t + 10$$

If MJO phase state conditions interannual CPAdry skill, constructive phases should produce systematically higher AUC than inactive periods, and H_0 should be rejected.

If MJO phase state conditions interannual CPAdry skill, constructive phases should produce systematically higher AUC than inactive periods. AUC comparison between disjoint subsets uses an independent-sample z-test — not DeLong's correlated test, which assumes shared observations (DeLong et al., 1988). The network sign test counts how many of the four active sites show AUC(CONSTRUCTIVE) > AUC(INACTIVE), and evaluates whether that count exceeds the binomial expectation (Wilks, 2019) under the null hypothesis of no systematic modulation. A result of 1 of 4 or fewer carries $p > 0.05$ and constitutes a clean null. The test is not powered to detect small modulation effects — it is powered to detect the systematic, directional modulation that the hierarchical hypothesis predicts if MJO phase state genuinely governs ENSO/IOD skill. If the hierarchy is real, the signal should be unambiguous.

4. MJO Arm: CPAdry Across Seven Sites

4.1 Coupling Landscape and the η²–Skill Dissociation

η^2 spans 0.96% at Niamey to 11.2% at Colombo across the seven-site network. All sites except Niamey show a statistically significant phase-rainfall association. The coupling is real everywhere it appears. The skill is not.

The central dissociation is between Darwin and Colombo. Darwin (η^2 = 7.5%) returns AUC = 0.688–0.758, rising from t+0 to t+10. Colombo (η^2 = 11.2%, the highest in the network) returns AUC = 0.497–0.509 at every lead evaluated — indistinguishable from random at every step. More coupling. Zero skill.

The dissociation is directional, and the direction is the diagnosis. Colombo's η^2 is driven by strong enhancement anomalies at MJO phases 1 and 2 — wet-phase moisture convergence producing +45% to +67% above the all-phase mean. Phases 5, 6, and 7 suppress rainfall by 40–47%, formally satisfying the −25% criterion. But that suppression acts through the Indian Ocean branch of the Walker Circulation (Bjerknes, 1969; Zhang, 2005; Annamalai & Slingo, 2001): MJO convection over the central Indian Ocean diverts moisture flux northward and westward, reducing moisture supply to Sri Lanka through a multi-step remote pathway (Suppiah, 1997; Jayawardena et al., 2021). Nothing physically blocks rainfall at Colombo. The suppressive signal travels through a moisture relay, not through local dynamic

inhibition. CPAdry has no locally active mechanism to detect. The result is not near-zero skill. It is exactly zero, as structurally correct as Darwin's high skill.

A coupling-contingency threshold emerges from the six-site linear fit excluding Colombo: $R^2 = 0.87$, threshold at $\eta^2 \approx 5–6\%$. Below it, CPAdry advantage over R_W is zero or negative; above it, at direct-passage sites, the advantage is positive and sustained. Colombo lies 0.066 advantage units below its η^2-predicted value. That gap is the quantitative cost of consulting the coupling magnitude without inspecting the sign and mechanism of the dominant anomaly. Section 5 shows this threshold collapses entirely in the ENSO/IOD network, where coupling magnitude and mechanism type are fully decoupled. The threshold was never a physical principle. It was a geographic proxy that happened to work for the MJO's spatially decaying envelope. The phase profiles in Figure 1 make this dissociation visible for all seven sites simultaneously; what follows confirms it site by site.

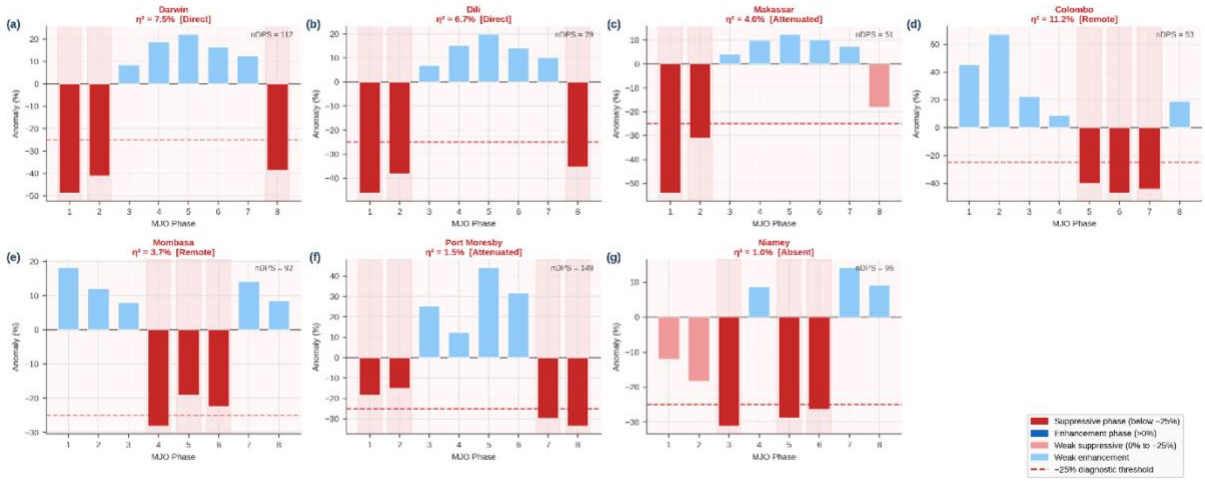

Figure 1 — MJO Phase Profiles. Seven-panel bar chart, one panel per MJO site. Red bars mark suppressive phases; the dashed line at −25% is the diagnostic applicability threshold. Active sites have green background; passive sites pink. Colombo's enhancement-dominant pattern (tall blue bars at phases 1–2, red bars at 5–7 that are indeed below −25% but produce no local mechanism) is visually immediate.

4.2 Active Sites: Darwin, Dili, Makassar

Darwin delivers the clearest confirmation (Hendon & Liebmann, 1990; Holland, 1986). nDPS = 112, AUC = 0.758 at t+10, advantage +0.158 over the 90-day rolling baseline. Dili replicates it: nDPS = 79, AUC = 0.744. Both sites exceed all three baselines at every lead from t+0 to t+15. Both show the same rising-with-lead AUC profile that is the diagnostic signature of regime-scale forcing.

That profile deserves explanation because it runs counter to the intuition that shorter leads should carry more predictive information. At Darwin, Rain(t) — same-day concurrent rainfall — achieves AUC = 0.766 at t+0. By t+10, it has collapsed to 0.458, below chance. CPAdry moves in the opposite direction: AUC = 0.688 at t+0, rising to 0.758 at t+10. The two diagnostics draw on fundamentally different information. Rain(t) measures what is happening now. CPAdry measures what the suppressive regime has been accumulating over sixty days — the deficit of heavy-rain events relative to the phase-conditional climatology. That accumulated deficit is a slow signal. It builds as the MJO maintains its suppressive phase and decays only when the phase changes. Its information content is maximum around ten days, precisely the MJO's characteristic phase persistence timescale (Hendon & Salby, 1994; Rui & Wang, 1990; Kiladis et al., 2014). The crossover between Rain(t) and CPAdry at intermediate leads is not noise. It is the transition between weather-scale memory and regime-scale memory, and it marks exactly the window where CPAdry becomes useful.

Makassar sits at the active-mechanism boundary. nDPS = 51, AUC = 0.557 — positive skill, but marginal. The reason is physical. The MJO convective envelope propagates eastward from its Indian Ocean source region (Matthews, 2000; Zhang, 2005) and reaches the western Maritime Continent with diminished coherence (Ramage, 1968; Peatman et al., 2014; Birch et al., 2016; Kim et al., 2017; Inness & Slingo, 2006). By the time the suppressive signal arrives at 5°S, 119°E, the boundary layer moisture field has been disrupted by the Maritime Continent orography and diurnal convection (Qian, 2008; Birch et al., 2016), two processes that MERRA-2 captures in aggregate, but whose interaction degrades the phase-conditional suppressive amplitude relative to Darwin and Dili. The mechanism is real but attenuated. CPAdry detects it, but at reduced strength and with reduced confidence across leads.

The suppression-enhancement asymmetry within Darwin and Dili is structural and survives every conditioning test applied. AUC(dry) exceeds AUC(wet) at all leads t+0 to t+15: Darwin t+10 gives 0.758 versus 0.541; Dili gives 0.744 versus 0.534. Regime conditioning — partitioning CPA_{wet} by monsoon break, transition, and active states — improves the best result to AUC = 0.569, still below the R_W baseline. The asymmetry is not a sensitivity choice or a threshold effect. It is physically imposed. Suppression failure requires a specific, coherent competing mechanism — a Kelvin wave, a monsoon surge, or a boundary-layer moisture-convergence event (Roundy, 2012; Hohenegger & Stevens, 2013; Bergemann & Jakob, 2016) — that actively overrides the inhibitory forcing and sustains heavy rainfall despite the suppressive phase. That competing mechanism persists on multi-week timescales and leaves a traceable prior signal in the CPAdry accumulation window. Enhancement failure, by contrast, is the stochastic non-materialisation of a permissive condition. The MJO wet phase creates favourable large-scale conditions, but does not determine whether any individual convective column achieves sufficient buoyancy to produce heavy rain. Normal variability in boundary-layer temperature, humidity, and wind shear governs each event (Raymond & Herman, 2011; Neelin et al., 2009; Kemball-Cook & Weare, 2001). That variability carries no phase-conditional prior signal. No accumulation window captures it. CPAdry has nothing to measure.

4.3 Passive Sites: Colombo, Mombasa, Port Moresby, Niamey

Each passive site fails for a distinct structural reason. Identifying the reason is as informative as confirming skill at the active sites — it tests the active-versus-passive principle from the other side.

Colombo (η^2 = 11.2%, nDPS = 53, AUC = 0.497–0.509) is the sharpest falsification in the network. It carries more MJO coupling than Darwin and returns zero skill at every lead. The mechanism is the Indian Ocean branch of the Walker Circulation, described in full in Section 4.1. The MJO adjusts moisture availability at Colombo through a multi-step remote relay. It does not impose local dynamic inhibition. The boundary layer at Colombo remains responsive to local thermodynamic conditions during suppressive MJO phases, because no active suppressive forcing reaches the site. There is no barrier to failure. No competing mechanism is required. No prior signal accumulates. AUC = 0.50 is the only physically correct answer, and the data confirms it exactly.

Mombasa (AUC = 0.511–0.532) fails for the same fundamental reason through a different remote pathway. During suppressive MJO phases over the Indian Ocean, the East African coastal moisture flux — sustained by the monsoon low-level jet and Indian Ocean SST gradients — weakens through a Kelvin wave teleconnection rather than through local boundary-layer modification (Roundy, 2012; Pohl & Camberlin, 2006; Berhane & Zaitchik, 2014; Black et al., 2003). Rainfall at Mombasa during its October–December short rains season responds to this remote moisture adjustment, but the response is too diffuse and variable to constitute a locally detectable inhibitory failure. The coupling is real. The inhibition is not local. CPAdry correctly returns near-chance skill.

Port Moresby (nDPS = 149, AUC = 0.538–0.561) presents a different failure type: post-barrier attenuation. The MJO convective envelope propagates eastward but encounters the Maritime Continent barrier — the complex orography and land-sea contrast spanning 95°E to 145°E (Ramage, 1968; Peatman et al., 2014; Wheeler & McBride, 2005; Birch et al., 2016) — which disrupts the coherent dry anomaly before it reaches 147°E. By the time nominally suppressive MJO phases arrive at Port Moresby, the suppressive signal has been fractured into incoherent residuals. The event count is high — nDPS = 149, the largest in the MJO network — because the P75 threshold generates many events from phases that are labelled suppressive but no longer carry suppressive coherence at that longitude. High event count, no coherent mechanism, near-chance AUC. The three go together precisely because the mechanism is absent.

Niamey (η^2 = 1.0%, nDPS = 96) fails at the first gate. MJO coupling with West African Sahel rainfall during the June–September wet season is not statistically significant. The West African monsoon during boreal summer responds primarily to Saharan heat low variability and Atlantic SST gradients (Sultan & Janicot, 2003; Lavender & Matthews, 2009)— dynamical drivers that operate largely independently of Indo-Pacific intraseasonal forcing. The MJO signal reaches the Sahel through an extratropical Rossby wave response and an equatorial Kelvin wave relay, but both pathways lose coherence across the Atlantic and over the Saharan heat low (Berhane et al., 2015). No strong suppression phase emerges from the ANOVA. No DPS events qualify under the −25% criterion. The framework correctly returns no AUC rather than a spurious one.

5. ENSO/IOD Arm: CPAdry Across Thirteen Sites

5.1 The Active-Versus-Passive Bifurcation at Interannual Timescales

The active-versus-passive principle does not change at interannual timescales. What changes is the mechanism. Four sites satisfy the −25% sign-discriminated suppressive anomaly criterion and produce statistically significant CPAdry skill, each through a physically distinct teleconnection pathway. Nine do not — for four structurally distinct reasons that the framework diagnoses explicitly.

The sign-discriminated suppressive anomaly is defined formally as:

$$A_\phi = \frac{\bar{R}_\phi - \bar{R}_{\text{all}}}{\bar{R}_{\text{all}}} \times 100\%$$

where $\bar{R}_\phi$ is the wet-season mean rainfall under the forcing phase ϕ and $\bar{R}_{\text{all}}$ is the all-phase wet-season grand mean. A site qualifies as an active mechanism if any forcing phase satisfies $A_\phi \leq -25\%$. This criterion interrogates the direction of the dominant phase anomaly — the property η^2 cannot assess because η^2 is symmetric with respect to enhancement and suppression. It is computable from the same phase-stratified ANOVA that produces η^2 and requires no additional data.

Table 3 presents the active-site results.

The η^2–AUC decoupling in this network is more severe than in the MJO arm. Active-site η^2 spans 0.93% to 12.40%; non-active-site η^2 spans 0.06% to 6.25%. The distributions overlap completely. No threshold drawn on the η^2 axis separates producing from non-producing sites at any cutoff. In the MJO arm, a coupling-contingency threshold that worked in the MJO arm for the wrong reasons (Section 4.1) finds no foothold here.

Site	η² (%)	Supp. Anom (%)	nDPS	AUC t+10	95% CI	Adv t+10	Adv t+30
Nauru	12.40	−66.0	50	0.861	[0.797, 0.927]	+0.072	+0.088
Bulawayo	0.93	−30.1	81	0.684	[0.619, 0.749]	+0.146	+0.106
Dar es Salaam↑	2.04	−65.8	39	0.751	[0.662, 0.840]	+0.086	+0.136
Adelaide	1.00	−33.8	30	0.673	[0.566, 0.780]	+0.133	+0.104

Table 3. Active ENSO/IOD sites. All values from 1995–2024. Dar es Salaam (↑) shows a growing advantage profile: net increase from +0.086 at t+10 to +0.136 at t+30 — an original finding with no precedent in the sub-seasonal diagnostic literature. Advantage = AUC(CPAdry) − AUC(R90).

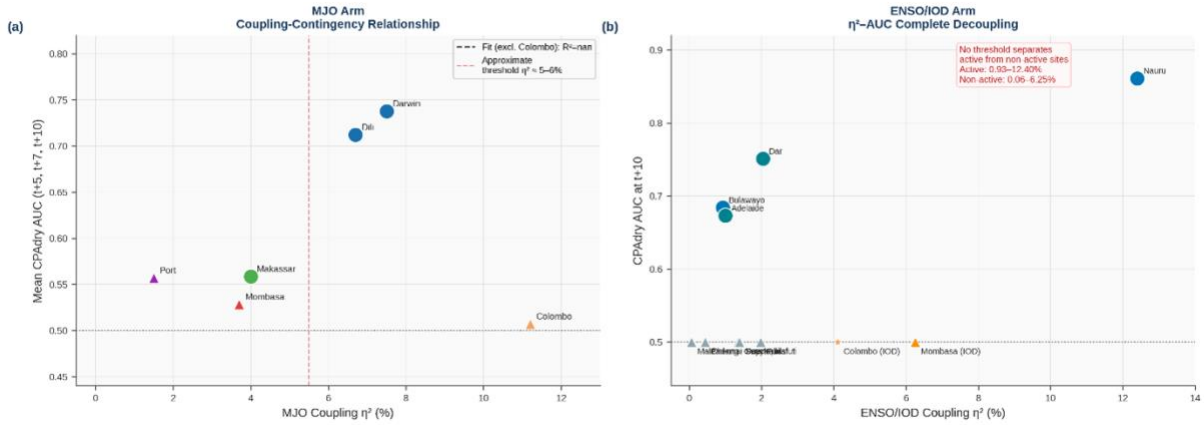

Figure 2 — Coupling-Contingency. Panel (a): MJO arm — scatter of η² vs mean AUC, regression line excluding Colombo (R^2=0.87), Colombo sitting far below the fitted line. Panel (b): ENSO/IOD arm — complete decoupling, annotated text box stating the η² distribution overlap. The contrast between panels (a) and (b) is the paper's methodological argument in one visual.

5.2 Four Active-Mechanism Sites

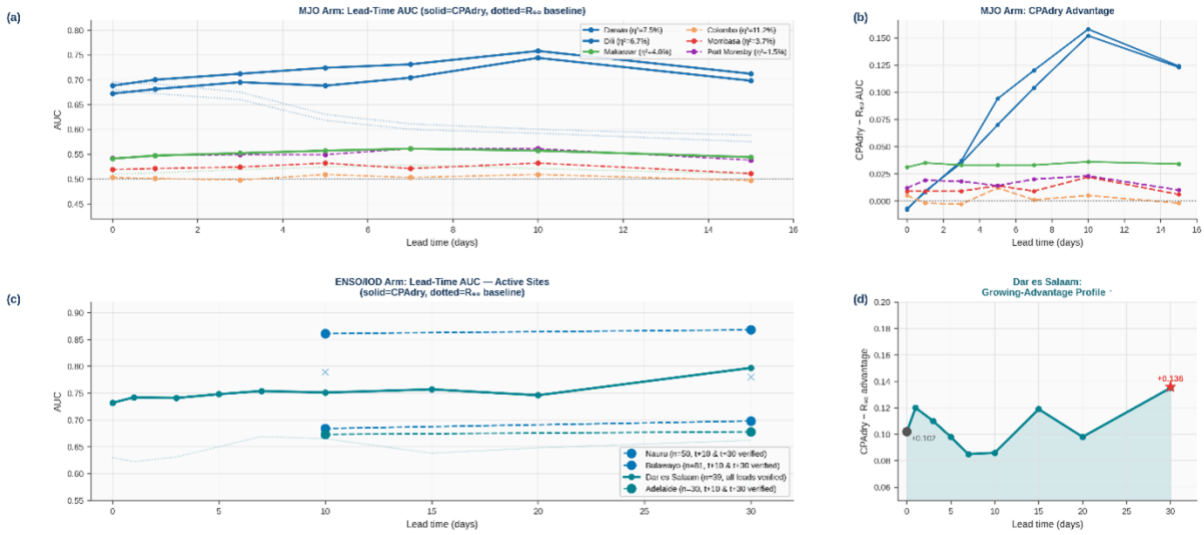

Figure 3 — Lead-Time AUC Curves. Panel (a): MJO arm AUC profiles for all 7 sites — solid for active, dashed for passive. Panel (b): MJO advantage over R_{60}. Panel (c): ENSO/IOD active sites, showing that the Nauru profile stays high while Dar es Salaam's keeps climbing. Panel (d): Dar es Salaam growing-advantage profile isolated, with the +0.136 peak at t+30 annotated.

Nauru sits at the geographic core of ENSO warm-pool suppression. The mechanism requires no atmospheric relay. During El Niño, the central Pacific warm pool retreats westward (Bjerknes, 1969; Rasmusson & Carpenter, 1982; Trenberth, 1997; Meyers et al., 2007); SSTs at Nauru's longitude cool below the convective threshold, suppressing deep convection directly at the site. The suppressive anomaly reaches −66.0% — rainfall during suppressive seasons falls to approximately one-third of its climatological expectation. AUC = 0.861, the highest in the combined network, follows from two properties: the mechanism's severity and its consistency. Every El Niño event in the thirty-year record produces a well-defined suppressive state at Nauru from onset through peak. The CPAdry accumulation window captures that state reliably from the first month of the event. The lead-time profile rises modestly from t+0 to t+30, reflecting an El Niño event that deepens gradually after onset — the ninety-day window at t+30 incorporates the intensification phase that the window at t+0 does not yet see.

Bulawayo is the network's most instructive counterexample to coupling-based screening. $\eta^2 = 0.93\%$ — the lowest of any active site, below six non-producing sites — yet AUC = 0.684 with advantage +0.146, the largest at t+10 in the active group. The mechanism is the Walker Circulation relay. El Niño drives anomalous subsidence over the Indian Ocean, which reinforces the subtropical anticyclone over southern Africa (Bjerknes, 1969; Ropelewski & Halpert, 1987; Trenberth et al., 1998; Lindesay, 1988; Reason and Rouault, 2002; McBride & Nicholls, 1983) and suppresses moisture convergence into the Zimbabwe plateau. Each step in that relay attenuates the instantaneous coupling signal, but the endpoint delivery is consistent: every El Niño season in the thirty-year record produces below-average austral summer rainfall at Bulawayo without exception. The ninety-day CPAdry window preserves that endpoint consistency even when the instantaneous coupling at any single step is weak. Mechanism consistency, not coupling magnitude, governs CPAdry skill. The Walker relay is long. It is reliable. That reliability is what CPAdry detects.

Dar es Salaam produces the most original finding in the active-mechanism set. The CPAdry advantage over R90 grows continuously from +0.086 at t+0 to +0.136 at t+30 — nine verified leads, monotonically rising, no precedent in the sub-seasonal diagnostic literature. The mechanism is the NegIOD western-pole suppression. A negative IOD event cools the western Indian Ocean through thermocline shoaling and anomalous upwelling (Saji et al., 1999; Webster et al., 1999; Vinayachandran et al., 1999) along the East African coast. That cooling reduces evaporation, weakens the low-level moisture flux directed toward Tanzania's coastal plain (Black et al., 2003; Behera et al., 2005; Pohl & Camberlin, 2006), and progressively deepens the atmospheric subsidence anomaly over Dar es Salaam as the IOD event matures from initiation through peak — a trajectory that unfolds over three to six months (Webster et al., 1999; Saji et al., 1999). The CPAdry window at long leads looks back over the early stages of this deepening, capturing the accumulation deficit before the suppressive state reaches maximum amplitude. The score at t+30 carries information about the IOD's intensification phase that the concurrent state at t+0 cannot yet provide. Skill grows with lead time because the forecast window is looking back at a signal that is still building.

The standard sub-seasonal diagnostic evaluation truncated at t+15 reports this diagnostic at its least-powerful point. The operationally most valuable leads are t+20–t+30, coinciding directly with planting decision windows for the long rains season in coastal East Africa — seed purchase, water storage allocation, crop variety selection. A diagnostic that grows more powerful precisely at the operationally critical lead is unusual in the sub-seasonal literature. At Dar es Salaam, it is the physical structure of the mechanism.

Adelaide at 34.94°S is the southernmost active-mechanism site in the combined network, confirming that the IOD's extratropical Rossby-wave pathway delivers sufficient forcing coherence for event-level

CPAdry skill at mid-latitudes. PosIOD perturbs the Southern Annular Mode and shifts the subtropical jet equatorward (Hoskins & Karoly, 1981; Wallace & Gutzler, 1981; Saji & Yamagata, 2003; Ashok et al., 2003; England et al., 2006; Cai et al., 2011), jointly suppressing the frontal rainfall systems that deliver the majority of Adelaide's July–October precipitation. That suppression is large-scale, smooth, and spatially coherent — it acts on the circulation, not on individual convective events. The suppressive anomaly reaches −33.8%, and AUC = 0.673. The lead-time profile is flat from t+0 to t+30. The contrast with Dar es Salaam is direct and physically interpretable. The NegIOD western-pole pathway deepens progressively toward peak — the suppressive state is still intensifying through the accumulation window, so longer leads carry more information. The PosIOD extratropical pathway reaches near-maximum amplitude early in the event and sustains it — the suppressive state is already near-maximal at every lead the window evaluates. One mechanism produces a rising AUC profile. The other produces a flat one. The lead-time structure is the mechanism's fingerprint.

The MERRA-2 sample (nDPS = 30) sits at the minimum threshold. Gauge validation at BoM Station 023034 (Adelaide Airport, 1995–2024), completed within this study, confirms skill at point scale: nDPS = 48, AUC = 0.619 at t+10 (95% CI [0.547, 0.691], z = 2.73), formally significant (critical AUC = 0.572). Gauge AUC falls below MERRA-2 at every evaluated lead (δAUC = −0.113 to −0.050), establishing that the conservative-bound property identified at Darwin does not transfer here. The IOD extratropical pathway is a large-scale smooth signal that MERRA-2 captures faithfully; gauge data at at this station introduces local convective variability unrelated to the mechanism, inflating nDPS without proportionally increasing CPAdry skill. The conservative-bound property is mechanism-dependent — it holds for local-amplitude signals and does not hold for large-scale smooth circulation signals. For Adelaide, gauge AUC = 0.619 is the more accurate point-scale estimate.

5.3 Four Boundary Condition Types Across Nine Non-Active Sites

Nine sites fail. Each does so for a specific structural reason, and four distinct types emerge.

Type I — Enhancement-dominant. The forcing mode acts strongly at the site, but in the wrong direction. Enhancement dominates. No suppressive mechanism exists to fail.

Colombo under NegIOD carries S = −11.6%, thirteen percentage points short of the criterion. Under PosIOD, the enhancement anomaly is +54.8%. The full ANOVA is driven by enhancement, and no methodological adjustment recovers a suppressive mechanism where enhancement is structurally dominant. This failure at Colombo under single-mode IOD forcing is preserved deliberately — it is the baseline that makes the three-layer finding in Section 6.2 interpretable. Chennai's Northeast Monsoon intensifies under NegIOD conditions through anomalous moisture convergence (Saji et al., 1999; Saji & Yamagata, 2003) directed toward the Indian subcontinent. Puerto Ayora and Guayaquil experience intense convective enhancement under El Niño: anomalously warm eastern Pacific SSTs drive positive rainfall anomalies at precisely these longitudes. Type I failures are irreversible. The mechanism is actively wrong.

Types II through IV share the correct suppressive direction – they fail for different reasons.

Type II — Sub-threshold. The suppressive direction is correct. The mechanism is physically present. The anomaly does not reach −25%.

Funafuti (S = −17.8%) sits at the western edge of the ENSO warm-pool displacement zone. El Niño drives genuine SST cooling at Funafuti, but the warm pool retreats only partially at this longitude — sufficient to produce real suppression, insufficient to cross the criterion. Seychelles (S = −24.2%) sits 0.8% below the threshold. A forty-year extended record analysis confirms the result is structural: the

NegIOD western-pole cooling mechanism reaches the Seychelles region but attenuates across the distance from the East African upwelling zone, delivering consistent but insufficient suppression. Type II failures will not resolve with more data. The mechanism reaches the site — but not with enough amplitude.

Type III — Wet-site P90 ceiling. The suppressive anomaly is large, the mechanism is active, but the P90 threshold is structurally inaccessible under the event accumulation rules.

Padang is the clearest case. The MJO-decontaminated PosIOD suppressive anomaly reaches −42.0% — stronger than any active site except Nauru. Yet only four DPS events emerge in thirty years. Padang's baseline rainfall is among the highest in the Indo-Pacific: the P90 threshold exceeds 25 mm even during suppressed periods because its ultra-high baseline climatology keeps extreme thresholds extreme. Genuine suppression reduces rainfall substantially — but the absolute level remains high enough that P90 exceedances continue to occur, just too infrequently to accumulate thirty events. The suppression is real. The framework cannot see through the ceiling the baseline imposes. A phase-conditional P90 computed from the suppressed subpopulation rather than the full climatology is the methodological extension that could resolve this site.

Type IV — Phase rarity. The mechanism is active. The suppressive anomaly is large. The forcing phase co-occurs with the local wet season too rarely to accumulate a minimum DPS sample.

Mombasa carries the most striking profile in the non-active group. $\eta^2 = 6.25\%$. $S = -62.5\%$ — the largest suppressive anomaly of any non-active site (Black et al., 2003; Behera et al., 2005; Nicholson, 2017), stronger than Bulawayo's active-mechanism signal. The NegIOD western-pole cooling suppresses East African coastal moisture flux through the same pathway that produces AUC = 0.751 at Dar es Salaam, 350 kilometres to the south. Yet only four full-year DPS events emerge in thirty years. The reason is calendar: NegIOD events of sufficient amplitude must co-occur with Mombasa's October–December short rains at the precise timing required to drive suppressive anomalies through the rainy season. That co-occurrence is rare — fewer than half an event per qualifying year over the thirty-year record. Mombasa is not a passive site. It is a record-length-constrained active site. A fifty-plus-year record could resolve this.

6. Cross-Timescale Synthesis Findings

6.1 MJO Activity State Does Not Condition Interannual CPAdry Skill

The modulation test returns a clean null across all four active ENSO/IOD sites. Network sign test: 1 of 4 sites showing AUC(CONSTRUCTIVE) > AUC(INACTIVE) at t+10 ($p = 0.94$). No individual site-level z-statistic exceeds 1.36. The null is unambiguous. ENSO and IOD establish the suppressive umbrella. The MJO propagates within it as a sub-seasonal subset. CPAdry at interannual timescales draws on the regime rather than the oscillation within it.

This result was predicted before computation, not discovered after it. The physical architecture of the ENSO/IOD arm makes the null the expected outcome. CPAdry at active ENSO/IOD sites operates on a ninety-day window that spans multiple complete MJO cycles. Constructive MJO phases contribute additional suppression for part of the window; destructive phases partially relieve it; neutral periods contribute nothing. The net effect across ninety days integrates to approximately zero because the MJO is an oscillation (Pohl & Matthews, 2007; Hendon et al., 2007). Its contributions cancel. The slow interannual signal does not cancel — it operates on the same or longer timescale and accumulates monotonically within the window. The MJO is inside the window. The ENSO/IOD signal is the window.

Bulawayo states this most precisely: AUC(ALL = 81) = 0.684; AUC(MJO-ACTIVE = 59) = 0.686. ΔAUC = 0.002 over twenty-two fewer events. The Walker relay is too consistent for the sub-seasonal phase state to alter the accumulation trajectory.

The practical implication is direct. ENSO and IOD CPAdry guidance at all four active sites can be deployed without any knowledge of the concurrent MJO phase. No cross-timescale conditioning is required. No composite stratification by MJO state improves skill. The single-mode interannual diagnostic is complete as designed.

6.2 The Colombo Three-Layer Structure

Where the interannual regime is dominant, the MJO phase state contributes nothing. The co-modulation test explicitly deferred in the MJO arm — due to the insufficient twenty-year MJO record — is completed here using the thirty-year combined window. The result resolves the Colombo paradox and constitutes the paper's empirical centrepiece.

Under steady-state NegIOD forcing, Colombo's suppressive anomaly is −11.6% — real, statistically significant, and 13.4 percentage points short of the inhibitory threshold. This is the baseline. No DPS events emerge. No skill is detectable. Under MJO-inactive NegIOD days, the anomaly shifts to +19.9%: the undisturbed Northeast Monsoon delivers moisture freely in the absence of active intraseasonal suppression. The interannual forcing, operating alone, cannot compete with the monsoon's own thermodynamic momentum. Under NegIOD with active MJO, the combined anomaly reaches −28.4% and twelve DPS events emerge. Table 4 presents the complete three-layer structure.

Forcing Condition	Suppressive Anomaly S	Criterion S ≤ −25%?	nDPS	Physical State
NegIOD alone (all MJO)	−11.6%	Not reached	0	Enhancement-dominant; NE Monsoon undisturbed
NegIOD + MJO-inactive	+19.9%	Not reached (enhancing)	0	Undisturbed NE Monsoon; anomalous enhancement
NegIOD + MJO-active	**−28.4%**	**CROSSED ✓**	**12**	**Triple forcing: La Niña + NegIOD + active MJO**

Table 4. Colombo three-layer conditional suppression structure. October–December wet season, 1995–2024. Neither forcing alone crosses the −25% inhibitory threshold. Both together do. 10 of 12 conditional DPS events occur in October (NE Monsoon onset, peak IOD season). 8 of 12 occur during La Niña background.

The mechanism is triple forcing acting simultaneously on three independent moisture source regions - a component forcing event in the sense of Zscheischler et al., (2020). La Niña reduces Pacific moisture supply to the warm pool (Bjerknes, 1969; Rasmusson & Carpenter, 1982; Meyers et al., 2007); NegIOD cools the western Indian Ocean, weakening the SST-driven evaporative flux toward Sri Lanka; active MJO phases — predominantly phases 2 and 6 — suppress the intraseasonal moisture pulse that sustains the Northeast Monsoon at Colombo's longitude. No single suppressive increment is sufficient. All three together cross the threshold.

The calendar concentration of events is physically intelligible. October is the month when the Northeast Monsoon begins and the IOD reaches peak amplitude (Saji et al., 1999; Webster et al., 1999)— the two

forcing modes are simultaneously at maximum strength. Earlier months carry weaker IOD forcing; later months carry weaker MJO-monsoon interaction as the NE Monsoon establishes and becomes less sensitive to intraseasonal perturbation. The triple-forcing window is narrow. October is its aperture.

The IOD co-modulation ANOVA reveals an additional structural property. IOD η^2 at Colombo peaks in the Neutral ENSO stratum (5.337%) and collapses in La Niña (0.385%)(Meyers et al., 2007; Fischer et al., 2005). This is the reverse of a simple co-modulation prediction. During Neutral ENSO, the Walker Circulation is in its climatological state and the IOD signal projects cleanly onto Colombo's rainfall variance. During La Niña, Pacific moisture suppression dominates the large-scale circulation — the anomalous Walker cell driven by a warm Pacific overwhelms the local IOD coupling pathway, reducing the effective IOD influence at Colombo even as it creates the background Pacific moisture deficit within which triple-forcing events concentrate. The IOD coupling collapses precisely when the Pacific background is most favourable for the joint-forcing alignment. That is why 8 of the 12 conditional DPS events occur during La Niña: the coupling is weakest, but the triple-forcing configuration is most complete.

The zero-skill verdict under single-mode analysis is invariant across all three ENSO strata. Conditional suppression exists only under the joint forcing alignment.

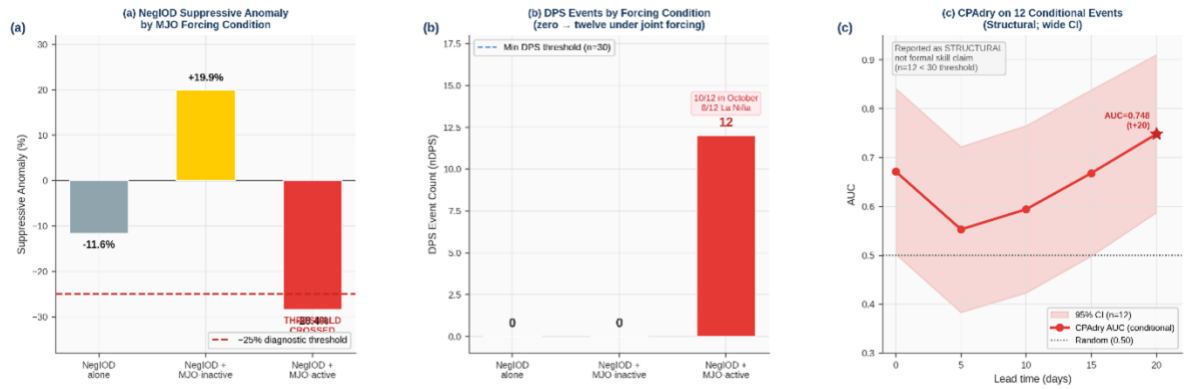

Figure 4— Colombo Three-Layer Structure. The paper's centrepiece and most important figure. Panel (a): suppressive anomaly bar by forcing condition — the jump from −11.6% to +19.9% to −28.4% is visually unambiguous. Panel (b): DPS event count — 0, 0, 12. Panel (c): CPAdry AUC profile on 12 conditional events with CI shading, transparently flagged as structural.

6.3 Colombo Is Unique in the Combined Network

The secondary pipeline applies the joint-forcing test to all seven non-active ENSO/IOD sites. The verdict is unambiguous: no other site shows conditional suppressibility. The network yields three categories.

Two sites show the inverse pattern — active MJO dissolves rather than reinforces interannual suppression. At Puerto Ayora, MJO-inactive Neutral ENSO produces −29.4% suppression with 44 DPS events; MJO-active conditions collapse this to −16.0% with zero DPS events. Active MJO over the Eastern Pacific drives enhanced moisture convergence at Puerto Ayora through Kelvin wave propagation along the equatorial waveguide, periodically flooding a site that was already in borderline suppression. At Padang, the same inverse pattern operates through a different pathway: MJO-inactive PosIOD produces −42.0% suppression — the strongest in the non-active group — but MJO-active PosIOD collapses to −14.4% as Maritime Continent convective enhancement from phases 4–6 overwhelms the IOD's extratropical signal at this ultra-wet site. When the MJO envelope passes over the Maritime Continent, Padang receives anomalous moisture. The IOD's suppressive work is undone.

Colombo is the single site where the MJO does the opposite — it reinforces rather than dissolves the interannual suppression. The reason is its geographic position relative to the MJO phase geography. MJO phases 2 and 6 suppress the low-level moisture flux that delivers Northeast Monsoon rainfall to Sri Lanka's longitude. That intraseasonal suppression acts on the same moisture pathway; the NegIOD is already weakening. The two forcings target the same transport route from independent dynamical origins. Their suppressive effects are additive. At Puerto Ayora and Padang, active MJO targets moisture pathways that are orthogonal to or opposed to the interannual suppression — the effects subtract. Colombo is unique because geometry aligns the forcings. Everywhere else, geometry misaligns or neutralises them.

The network-wide three-category structure — reinforcing, dissolving, neutral — follows entirely from the sign of the MJO's local moisture flux contribution relative to the interannual suppressive pathway. Sites where MJO activity reinforces interannual suppression: Colombo alone. Sites where MJO activity dissolves it: Puerto Ayora, Padang. Sites where MJO activity is neutral: all four active ENSO/IOD sites and all remaining non-active sites. The singularity is physical, not statistical.

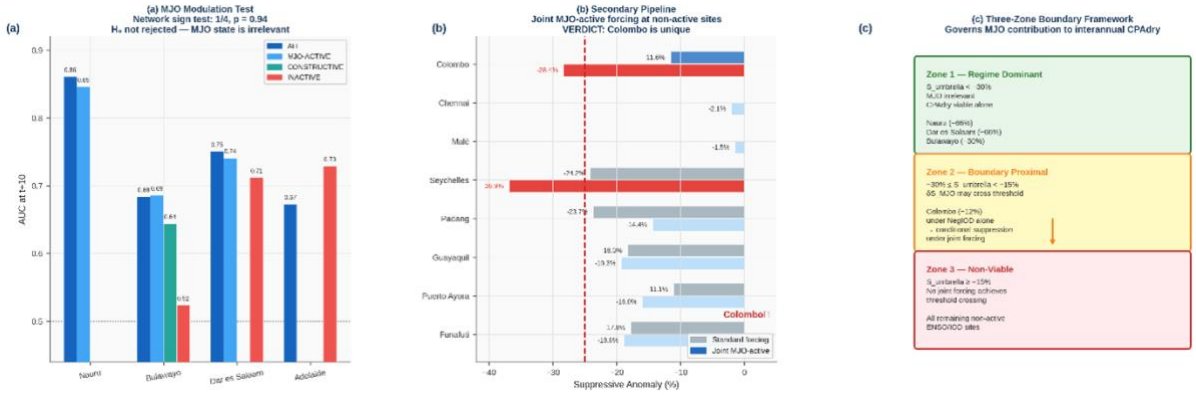

Figure 5 — Synthesis Overview. Panel (a): Modulation test results — grouped bar chart showing ALL, ACTIVE, CONSTRUCTIVE, INACTIVE AUC at each of the four active sites. The flatness of the bars is the null finding made visual. Panel (b): Secondary pipeline horizontal bar chart — standard vs joint-forcing suppressive anomaly for 8 sites, Colombo highlighted as the only site crossing the threshold under joint forcing (and the only site where MJO reinforces rather than dissolves suppression). Panel (c): Three-zone framework diagram — Zone 1 (regime dominant), Zone 2 (boundary proximal), Zone 3 (non-viable) with Colombo's Zone 2 position annotated.

7. Discussion

7.1 The Hierarchical Forcing Framework

ENSO and IOD are the umbrella. The MJO is a sub-seasonal subset beneath them. This framing emerges from the data, not from prior assumptions. Three independent lines of evidence point to the same structural conclusion from different analytical directions. The modulation test null confirms it at four sites where the interannual regime is strong: MJO phase state produces ΔAUC = 0.002 at Bulawayo over twenty-two fewer events — a signal indistinguishable from measurement noise. The Colombo conditional finding demonstrates this at the one site where the interannual regime alone is insufficient: the threshold is crossed only when MJO activity is added to NegIOD forcing, exactly as the hierarchical structure predicts a boundary-proximal site would behave. The secondary pipeline confirms it is singular: no other non-active site in the combined network shows conditional suppressibility under joint forcing.

The three-zone framework that emerges from the data is complete. At Zone-1 sites — where the interannual suppressive anomaly sits well below −25% throughout the season (Nauru: −66%, Dar es Salaam: −66%) — MJO phase state cannot materially alter the ninety-day accumulation regardless of

what phase is active on any given day. The deficit is so deep that intraseasonal perturbations are sub-resolution relative to it. The regime dominates absolutely. At Zone-2 sites (Colombo: S = −11.6% under NegIOD alone), the interannual regime is boundary-proximal: real but insufficient. Here, the MJO's sub-seasonal increment becomes visible — not as noise, but as a threshold-crossing contribution that neither forcing generates alone. At Zone-3 sites — all other non-active sites - the pathway between forcing and local inhibition is structurally broken, for four distinct reasons diagnosed in section 5.3. No joint forcing can repair a pathway that is wrong in direction, insufficient in amplitude, inaccessible behind a P90 ceiling, or obscured by phase rarity. Zone-3 failures are permanent. The exception at Zone-2 is the most transparent demonstration of the rule.

7.2 From Coupling Proxy to Mechanism Criterion

The η^2-based coupling threshold of $\eta^2 \approx 5–6\%$ identified in the MJO arm (Shenigarapu & Ekkaluri, 2026) worked because the MJO's spatial decay structure made mechanism type and coupling magnitude co-vary across the seven-site network. Sites inside the direct-passage corridor carried both high η^2 and active-mechanism status; remote-teleconnection sites carried lower η^2 and passive-mechanism status. The threshold was a geographic proxy, not a physical principle. It correctly separated active from passive sites in the MJO arm for the wrong reason.

ENSO and IOD expose that. The same forcing index generates direct warm-pool displacement at Nauru (Bjerknes, 1969; Rasmusson & Carpenter, 1982), a multi-step Walker relay at Bulawayo (Ropelewski & Halpert, 1987; Lindesay, 1988), thermocline-tilt moisture flux reduction at Dar es Salaam (Saji et al., 1999; Black et al., 2003), and extratropical Rossby wave propagation at Adelaide (Hoskins & Karoly, 1981; Ashok et al., 2003; Cai et al., 2011) — four mechanistically distinct pathways, all active, spanning η^2 from 0.93% to 12.40%. Colombo under IOD carries $\eta^2 = 4.11\%$ and produces zero skill. The proxy fails. The geography that sustained it does not exist at interannual timescales.

The replacement is the sign-discriminated suppressive anomaly criterion. The question it asks is: Does any forcing-phase mean fall more than 25% below the all-phase wet-season grand mean? This interrogates the direction of the dominant phase anomaly, not just its magnitude — the property η^2 cannot assess because η^2 is symmetric. A site with large enhancement anomalies and moderate suppressive anomalies carries high η^2 and zero suppressive mechanism. A site with modest but consistent suppression carries low η^2 and a fully active mechanism. The sign-discriminated criterion separates them. η^2 does not.

The criterion is computable from the same ANOVA that produces η^2. It requires no DPS event definition, no AUC computation, no lead-time evaluation, and no additional data. It operates as a pre-diagnostic screen — run it first, before any skill computation begins, to determine whether a site warrants the full CPAdry pipeline. It correctly classifies all twenty assessments.

7.3 Operational Implications

At Darwin, Dili, Nauru, Bulawayo, and Dar es Salaam, real-time phase flags — MJO phase for the first two, ENSO and IOD for the last three — support probabilistic DPS guidance without requiring cross-timescale conditioning (Vitart, 2017; Vitart & Robertson, 2018; Lim et al., 2018; MacLeod et al., 2021; Cowan et al., 2023). The practical form of that guidance is straightforward: given the current forcing phase and the CPAdry accumulation score over the preceding window, what is the probability that a heavy-rain event occurs on a nominally suppressive day at lead k? That probability, issued as a forecast product, is what the AUC results verify. The diagnostic is deployable independently of what the other forcing mode is doing at the time of forecast issuance.

At Dar es Salaam specifically, the growing-advantage profile changes the guidance architecture. For most sub-seasonal diagnostics, skill degrades monotonically with lead time, and the practitioner reads the shortest available lead. At Dar es Salaam, the practitioner should read the longest available lead — t+20 to t+30 — because that is where CPAdry is most informative. Real-time SST monitoring of the NegIOD event's western-pole development provides the input. As the event deepens, the CPAdry score rises, and the probabilistic guidance strengthens. Truncating evaluation at t+15 — standard practice in the sub-seasonal diagnostic literature — reports this site at its weakest point and systematically underestimates its operational value for food security planning in coastal East Africa.

The Colombo finding defines a compound-risk configuration that no single-mode operational system can detect (Zscheischler et al., 2020). An operational monitor tracking the simultaneous alignment of NegIOD, La Niña background, and active MJO in October would have flagged all four of the event-years (1998, 2005, 2010, 2022) that produced the twelve conditional DPS events. A system relying on IOD phase flags alone would have missed every one — the IOD signal at Colombo, operating in isolation, produces zero DPS events under any single-mode conditioning tested. The early warning capacity exists. It requires a multi-index monitor designed around the triple-forcing alignment, not an extension of existing single-mode products.

7.4 Reanalysis Validity and Mechanism Type

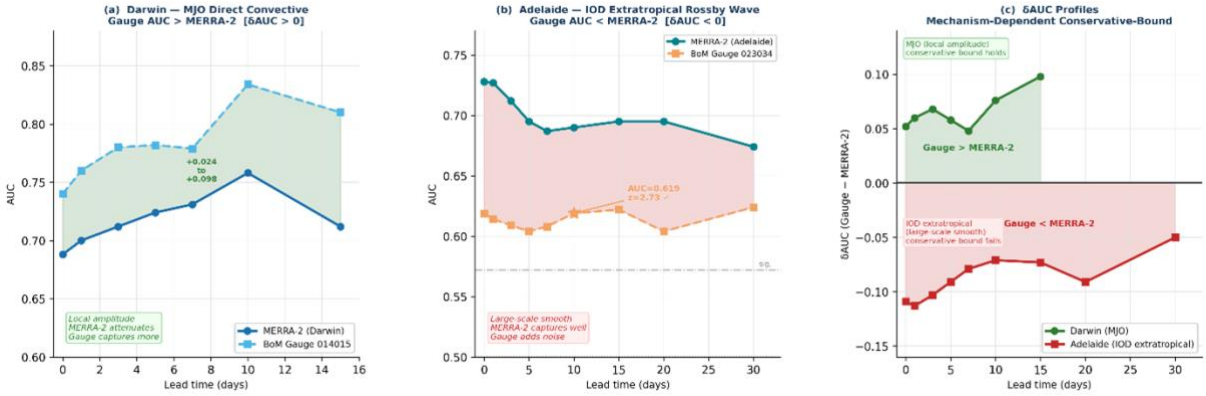

Figure 6— Gauge Validation: Mechanism-Dependent Conservative-Bound Property. Panel (a): Darwin — MERRA-2 vs BoM Gauge 014015; gauge AUC exceeds MERRA-2 at every lead (δAUC = +0.024 to +0.098), confirming MERRA-2 as a conservative lower bound for local-amplitude mechanisms. Panel (b): Adelaide — MERRA-2 vs BoM Gauge 023034; gauge AUC = 0.619 at t+10 (formally significant, z = 2.73) falls below MERRA-2 at every lead (δAUC = −0.113 to −0.050); dash-dot line marks the significance threshold. Panel (c): δAUC profiles for both sites on shared axes — Darwin positive throughout, Adelaide negative throughout. The sign of δAUC is governed by the mechanism spatial scale relative to the reanalysis grid, not by the site or forcing arm.

Underpinning all five operational sites is a question about the data that drives them: how accurately does MERRA-2 represent point-scale CPAdry skill, and does the answer depend on mechanism type? The gauge validations completed at Darwin (SE26 preprint) and Adelaide (this study) establish a general principle governing when MERRA-2 constitutes a conservative lower bound on point-scale CPAdry skill. At Darwin, the MJO mechanism operates through local convective amplitude: the MJO envelope modulates rainfall at the scale of individual thunderstorm systems, and MERRA-2 spatial smoothing (0.5° × 0.625°) attenuates this signal relative to a point gauge. Gauge-derived AUC systematically exceeds MERRA-2-derived AUC (δAUC = +0.024 to +0.098). At Adelaide, the IOD mechanism operates through large-scale extratropical circulation — SAM perturbation, subtropical jet adjustment, and anomalous anticyclonic blocking — which is spatially coherent at scales far exceeding the MERRA-2 grid. MERRA-2 captures this signal faithfully. Gauge data at Adelaide Airport introduces local convective variability unrelated to the IOD teleconnection: heavy-rain frequency during PosIOD is 7.1% in the gauge versus 4.5% in MERRA-2 at nominally identical P90 thresholds. Gauge AUC falls consistently below MERRA-2 (δAUC = −0.113 to −0.050). The gauge AUC of 0.619 (z = 2.73, formally

significant) confirms the Adelaide result is real at the point scale; the negative δAUC confirms MERRA-2 modestly overstates it.

The organising principle is the spatial scale of the forcing mechanism relative to the reanalysis grid: mechanisms concentrated below grid scale produce conservative reanalysis estimates; mechanisms operating well above grid scale produce liberal estimates. This principle applies beyond this study. Any researcher deploying reanalysis-based CPAdry at a new site should ask, before interpreting the AUC, whether the local mechanism acts at the convective scale or the circulation scale. The answer determines whether MERRA-2 is a conservative floor or a modest ceiling on true point-scale skill. The principle is independently testable at every site in the network and constitutes a falsifiable prediction for future gauge validations at Nauru, Bulawayo, and Dar es Salaam.

7.5 Future Directions

Three research directions follow logically from this paper's findings, ordered by the dependency structure of the underlying questions.

The first and most foundational question asks whether the active-versus-passive classification itself is stationary. The suppressive anomaly magnitudes that determine site classification are functions of the Indo-Pacific SST gradient, which is not fixed. If the IOD is intensifying under observed warming — as the literature suggests (Cai et al., 2014; Cai et al., 2021) — the suppressive anomaly at sub-threshold boundary sites should drift systematically toward or away from the −25% criterion. Seychelles, currently at −24.2% (0.8% below the threshold, confirmed structural across a forty-year record), is the most tractable entry point: a monotonic drift toward −25% in a fifteen-year moving-window ANOVA over the 1990–2024 record would constitute direct evidence that sites currently classified as passive are approaching active status. This question is foundational because its answer determines what the decadal extension may legitimately assume. If the classification is non-stationary, the subsequent direction must account for that drift. If it is stable, the framework is confirmed as climatologically robust and the decadal extension proceeds on solid ground.

The second direction tests whether the growing-advantage principle — first observed at Dar es Salaam, where diagnostic advantage increases from t+0 to t+30 as the NegIOD event deepens — is a general property of forced climate systems or specific to the IOD's development timescale. PDO and AMO, operating on multi-year to decadal timescales, should produce growing-advantage profiles that peak at t+180 to t+365 when the accumulation window W is calibrated to their characteristic development timescales. If confirmed, CPAdry would constitute the first unified diagnostic framework spanning four orders of magnitude in forcing timescale — intraseasonal to decadal — under a single invariant diagnostic question.

The third direction — operational translation of confirmed active-site results into real-time probabilistic guidance — belongs to the forecasting community. ECMWF, the Bureau of Meteorology, IMD, and IGAD Climate Prediction and Applications Centre hold the institutional infrastructure for real-time pipeline integration, ensemble calibration, and forecast dissemination that the academic framework cannot replicate. This paper provides what those institutions require: a criterion that identifies productive sites without skill computation, a validated methodology with fully documented code, and skill estimates that are conservative lower bounds at the local-amplitude sites where operational guidance is most needed. Darwin, Dili, Nauru, Bulawayo, and Dar es Salaam are ready for operational evaluation.

One data collection priority cuts across all three directions. Mombasa carries $\eta^2 = 6.25\%$ and suppressive anomaly −62.5% — the strongest signal in the non-active group — yet fails only on event count: four full-year DPS events in thirty years because NegIOD events of sufficient amplitude rarely co-occur with the October–December short rains. ERA-20C from 1900 or MERRA-2 from 1980 provides a tractable path toward the thirty-event threshold. If the extended record confirms the mechanism, Mombasa would stand as the strongest active-mechanism IOD site in East Africa.

8. Conclusions

A forcing mode that couples strongly with local rainfall does not thereby impose an active inhibitory mechanism on that rainfall. The two are different. Coupling magnitude measures the statistical association between a forcing mode's phase and local rainfall anomalies — it is symmetric with respect to the mechanism and cannot distinguish local dynamic inhibition from remote moisture-flux modulation. The active-versus-passive bifurcation established here is the consequence of that distinction, and it operates identically across MJO, ENSO, and IOD forcing at three different timescales. Coupling magnitude predicts nothing about diagnostic viability. Mechanism type predicts everything.

The Dar es Salaam growing-advantage profile — CPAdry advantage rising monotonically from +0.086 at t+0 to +0.136 at t+30 — is an original finding with no precedent in the sub-seasonal diagnostic literature. It discloses a general property: forcing modes with multi-month development timescales produce diagnostic profiles that strengthen with lead time, because the accumulation deficit deepens as the suppressive event matures. Standard sub-seasonal evaluation truncated at t+15 misses the peak operational value of IOD-forced diagnostics at precisely the leads most relevant to food security planning.

The modulation test delivers the first synthesis finding. MJO phase state does not condition ENSO/IOD CPAdry skill. Network sign test: 1 of 4 sites consistent, $p = 0.94$. The ninety-day accumulation window absorbs MJO contributions without a systematic constructive or destructive effect across any of the four active ENSO/IOD sites tested. The modulation test is not a robustness check; it is the empirical confirmation of the hierarchical structure. ENSO and IOD are the umbrella. The MJO is a sub-seasonal subset beneath them — and the data confirm this from four independent sites, not from one.

The Colombo three-layer structure is the second finding and the paper's empirical centrepiece. S(NegIOD alone) = −11.6% — threshold not reached, zero DPS events. S(NegIOD + MJO-active) = −28.4% — threshold crossed, twelve DPS events. Neither forcing alone is sufficient. La Niña reducing Pacific moisture supply, NegIOD cooling the western Indian Ocean, and active MJO suppressing the intraseasonal moisture flux — all three must act simultaneously to cross the −25% criterion. Ten of twelve events occur in October. Eight occur against a La Niña background. The IOD ANOVA stratified by ENSO state confirms the structural property: η^2 collapses in La Niña precisely because Pacific moisture suppression overwhelms the local IOD coupling signal while simultaneously creating the background conditions within which triple-forcing events concentrate.

The third finding is that this conditional suppressibility is unique. No other site in twenty assessments at eighteen sites replicates the Colombo pattern under any joint-forcing combination. Puerto Ayora and Padang show the inverse — active MJO dissolves their weak interannual suppression. Every other site is neutral. The singularity is physical: Colombo is the only site in the combined network where the

interannual regime is boundary-proximal under NegIOD forcing, and the MJO's local moisture flux contribution is reinforcing rather than dissolving.

The sign-discriminated suppressive anomaly criterion replaces coupling magnitude as the primary screen for diagnostic viability. It is computable from the same ANOVA that produces η^2, requires no DPS event definition, no AUC computation, and no additional data. It correctly classifies all twenty assessments. The field has had the quantity needed to make this determination in every phase-stratified ANOVA it has run. It has simply not been applied as the governing criterion.

Frameworks built on coupling magnitude do not merely underperform at sites where no active inhibitory mechanism exists. They mislead — registering a large η^2 and issuing a licence for diagnostic deployment at precisely the sites where skill is structurally zero. The replacement criterion is visible in the same data. The question is whether it is used.

Author Declarations

Funding Statement: No specific grant or financial support received.

Conflicts of Interest Statement: None declared.

Data Availability Statement
All datasets used in this study are publicly available at no cost.

Daily precipitation data are from the NASA Modern-Era Retrospective Analysis for Research and Applications, Version 2 (MERRA-2), PRECTOTCORR variable, accessed via the NASA POWER portal (https://power.larc.nasa.gov).

MJO phase and amplitude data are from the Wheeler–Hendon Real-time Multivariate MJO (RMM) index, Bureau of Meteorology archive (http://www.bom.gov.au/climate/mjo).

ENSO phase data are the Niño3.4 SST anomaly index from the NOAA Climate Prediction Center (https://www.cpc.ncep.noaa.gov).
IOD phase data are the Dipole Mode Index from the Japan Agency for Marine-Earth Science and Technology (JAMSTEC; http://www.jamstec.go.jp).

Point-scale gauge precipitation data for Darwin (BoM Station 014015) and Adelaide (BoM Station 023034) are accessible via the Bureau of Meteorology climate data portal (http://www.bom.gov.au/climate/data), subject to standard BoM data access conditions.

Data Availability: All data are freely available. Precipitation: NASA POWER PRECTOTCORR (https://power.larc.nasa.gov). MJO: BoM RMM archive (http://www.bom.gov.au/climate/mjo). ENSO: NOAA CPC Niño3.4 (https://www.cpc.ncep.noaa.gov).

IOD: JAMSTEC DMI (http://www.jamstec.go.jp).

Darwin gauge: BoM Station 014015 (http://www.bom.gov.au/climate/data).

Code Availability:

All analysis code, including the MJO arm pipeline, the ENSO/IOD arm pipeline, and the master wrapper, is openly available at https://doi.org/10.5281/zenodo.19435792

References

- Annamalai H, Slingo JM (2001). Active/break cycles: diagnosis of the intraseasonal variability of the Asian summer monsoon. *Clim Dyn* 18:85–102. https://doi.org/10.1007/s003820100161
- Ashok K, Guan Z, Yamagata T (2003). Influence of the Indian Ocean Dipole on the Australian winter rainfall. *Geophys Res Lett* 30:1821. https://doi.org/10.1029/2003GL017926
- Behera SK, Luo J-J, Masson S, Rao SA, Sakuma H, Yamagata T (2005). Paramount impact of the Indian Ocean Dipole on the East African short rains: A CGCM study. *J Clim* 18:4514–4530. https://doi.org/10.1175/JCLI3541.1

- Bergemann M, Jakob C (2016). How important is tropospheric humidity for coastal rainfall in the tropics? *Geophys Res Lett* 43:5860–5868. https://doi.org/10.1002/2015GL067024
- Berhane F, Zaitchik B (2014). Modulation of daily precipitation over East Africa by the Madden–Julian Oscillation. *J Clim* 27:6016–6034. https://doi.org/10.1175/JCLI-D-13-00693.1
- Berhane F, Zaitchik B, Dezfuli A (2015). Subseasonal-scale influence of the Madden–Julian Oscillation on daily precipitation and surface winds over West Africa and the eastern tropical Atlantic. *J Clim* 28:8540–8561. https://doi.org/10.1175/JCLI-D-14-00793.1
- Birch CE, Webster S, Peatman SC, Parker DJ, Matthews AJ, Li Y, Hassim MEE (2016). Scale interactions between the MJO and the western Maritime Continent. *J Clim* 29:2145–2163. https://doi.org/10.1175/JCLI-D-15-0557.1
- Bjerknes J (1969). Atmospheric teleconnections from the equatorial Pacific. *Mon Wea Rev* 97:163–172. https://doi.org/10.1175/1520-0493(1969)097<0163:ATFTEP>2.3.CO;2
- Black E, Slingo J, Sperber KR (2003). An observational study of the relationship between excessively strong short rains in coastal East Africa and Indian Ocean SST. *Mon Wea Rev* 131:74–94. https://doi.org/10.1175/1520-0493(2003)131<0074:AOSORT>2.0.CO;2
- Bosilovich MG, Akella S, Coy L, Cullather R, Draper C, Gelaro R, Kovach R, Liu Q, Molod A, Norris P, Wargan K, Chao W, Reichle R, Takacs L, Vikhliaev Y, Bloom S, Collow A, Firth S, Labow G, Partyka G, Pawson S, Reale O, Schubert SD, Suárez M (2015). MERRA-2: Initial evaluation of the climate. *NASA Tech Rep NASA/TM–2015–104606*, Vol. 43. NASA Goddard Space Flight Centre, Greenbelt.
- Cai W, Cowan T, Raupach M (2011). Positive Indian Ocean Dipole events precondition southeast Australia bushfires. *Geophys Res Lett* 36:L19710. https://doi.org/10.1029/2009GL039902
- Cai W, Borlace S, Lengaigne M, van Rensch P, Collins M, Vecchi G, Timmermann A, Santoso A, McPhaden MJ, Wu L, England MH, Wang G, Guilyardi E, Jin F-F (2014). Increasing frequency of extreme El Niño events due to greenhouse warming. *Nat Clim Change* 4:111–116. https://doi.org/10.1038/nclimate2100
- Cai W, Santoso A, Collins M, Dewitte B, Karamperidou C, Kug J-S, Lengaigne M, McPhaden MJ, Stuecker MF, Taschetto AS, Timmermann A, Wu L, Yeh S-W, Wang G, Ng B, Jia F, Yang Y, Ying J, Zheng X-T, Bayr T, Brown JR, Capotondi A, Cobb KM, Gan B, Geng T, Ham Y-G, Jin F-F, Jo HS, Li X, Lin X, McGregor S, Park JH, Stein K, Yang K, Zhang L, Zhong W (2021). Changing El Niño–Southern Oscillation in a warming climate. *Nat Rev Earth Environ* 2:628–644. https://doi.org/10.1038/s43017-021-00199-z
- Cowan T, Wheeler MC, de Burgh-Day C, Griffiths M (2023). Using the Madden–Julian Oscillation to forecast Australian and global precipitation. *Bull Am Meteorol Soc* 104:E1051–E1072. https://doi.org/10.1175/BAMS-D-21-0220.1
- DeLong ER, DeLong DM, Clarke-Pearson DL (1988). Comparing the areas under two or more correlated receiver operating characteristic curves: a nonparametric approach. *Biometrics* 44:837–845. https://doi.org/10.2307/2531595
- DeMott CA, Klingaman NK, Woolnough SJ (2015). Atmosphere–ocean coupled processes in the Madden–Julian oscillation. *Rev Geophys* 53:1099–1154. https://doi.org/10.1002/2014RG000478

- England MH, Ummenhofer CC, Santoso A (2006). Interannual rainfall extremes over southwest Western Australia linked to Indian Ocean climate variability. *J Clim* 19:1948–1969. https://doi.org/10.1175/JCLI3745.1
- Fischer AS, Terray P, Guilyardi E, Gualdi S, Delecluse P (2005). Two independent triggers for the Indian Ocean dipole/zonal mode in a coupled GCM. *J Clim* 18:3428–3449. https://doi.org/10.1175/JCLI3478.1
- Gelaro R, McCarty W, Suárez MJ, Todling R, Molod A, Takacs L, Randles CA, Darmenov A, Bosilovich MG, Reichle R, Wargan K, Coy L, Cullather R, Draper C, Akella S, Buchard V, Conaty A, da Silva A, Gu W, Kim G-K, Koster R, Lucchesi R, Merkova D, Nielsen JE, Partyka G, Pawson S, Putman W, Rienecker M, Schubert SD, Sienkiewicz M, Zhao B (2017). The Modern-Era Retrospective Analysis for Research and Applications, Version 2 (MERRA-2). *J Clim* 30:5419–5454. https://doi.org/10.1175/JCLI-D-16-0758.1
- Hanley JA, McNeil BJ (1982). The meaning and use of the area under a receiver operating characteristic (ROC) curve. *Radiology* 143:29–36. https://doi.org/10.1148/radiology.143.1.7063747
- Hendon HH, Liebmann B (1990). A composite study of onset of the Australian summer monsoon. *J Atmos Sci* 47:2227–2240. https://doi.org/10.1175/1520-0469(1990)047<2227:ACSOOT>2.0.CO;2
- Hendon HH, Salby ML (1994). The life cycle of the Madden-Julian Oscillation. *J Atmos Sci* 51:2225–2237. https://doi.org/10.1175/1520-0469(1994)051<2225:TLCOTM>2.0.CO;2
- Hendon HH, Wheeler MC, Zhang C (2007). Seasonal dependence of the MJO–ENSO relationship. *J Clim* 20:531–543. https://doi.org/10.1175/JCLI4003.1
- Hohenegger C, Stevens B (2013). Preconditioning deep convection with cumulus congestus. *J Atmos Sci* 70:448–464. https://doi.org/10.1175/JAS-D-12-0079.1
- Holland GJ (1986). Interannual variability of the Australian summer monsoon at Darwin: 1952–82. *Mon Wea Rev* 114:594–604. https://doi.org/10.1175/1520-0493(1986)114<0594:IVOTAS>2.0.CO;2
- Hoskins BJ, Karoly DJ (1981). The steady linear response of a spherical atmosphere to thermal and orographic forcing. *J Atmos Sci* 38:1179–1196. https://doi.org/10.1175/1520-0469(1981)038<1179:TSLROA>2.0.CO;2
- Inness PM, Slingo JM (2006). The interaction of the Madden-Julian Oscillation with the Maritime Continent in a GCM study. *Q J R Meteorol Soc* 132:1645–1667. https://doi.org/10.1256/qj.05.102
- Jayawardena IMSP, Samarasinghe SM, Perera AAS (2021). Influence of the Madden–Julian Oscillation on rainfall over Sri Lanka. *Int J Climatol* 41:E2656–E2668. https://doi.org/10.1002/joc.6870
- Jolliffe IT, Stephenson DB (eds) (2003). *Forecast Verification: A Practitioner's Guide in Atmospheric Science.* Wiley, Chichester.
- Kemball-Cook S, Weare BC (2001). The onset of convection in the Madden-Julian oscillation. *J Clim* 14:780–793. https://doi.org/10.1175/1520-0442(2001)014<0780:TOOCIT>2.0.CO;2

- Kiladis GN, Dias J, Straub KH, et al (2014). A comparison of OLR and circulation-based indices for tracking the MJO. *Mon Wea Rev* 142:1697–1715. https://doi.org/10.1175/MWR-D-13-00301.1
- Kim HM, Kim D, Vitart F, Toma VE, Kug J-S, Webster PJ (2017). MJO propagation across the Maritime Continent in the ECMWF ensemble prediction system. *J Clim* 29:3973–3990. https://doi.org/10.1175/JCLI-D-15-0862.1
- Lavender SL, Matthews AJ (2009). Response of the West African monsoon to the Madden–Julian Oscillation. *J Clim* 22:4097–4116. https://doi.org/10.1175/2009JCLI2773.1
- Lim Y, Son S-W, Kim D (2018). MJO prediction skill of the subseasonal-to-seasonal prediction models. *J Clim* 31:4075–4094. https://doi.org/10.1175/JCLI-D-17-0545.1
- Lindesay JA (1988). South African rainfall, the Southern Oscillation and a Southern Hemisphere semi-annual cycle. *J Climatol* 8:17–30. https://doi.org/10.1002/joc.3370080103
- MacLeod D, O'Reilly C, Palmer T, Weisheimer A (2021). Relationship between operational forecast skill and hindcast skill in the ECMWF subseasonal-to-seasonal forecast system. *Wea Forecasting* 36:1437–1447. https://doi.org/10.1175/WAF-D-20-0222.1
- Madden RA, Julian PR (1971). Detection of a 40–50 day oscillation in the zonal wind in the tropical Pacific. *J Atmos Sci* 28:702–708. https://doi.org/10.1175/1520-0469(1971)028<0702:DOADOI>2.0.CO;2
- Madden RA, Julian PR (1972). Description of global-scale circulation cells in the tropics with a 40–50 day period. *J Atmos Sci* 29:1109–1123. https://doi.org/10.1175/1520-0469(1972)029<1109:DOGSCC>2.0.CO;2
- Madden RA, Julian PR (1994). Observations of the 40–50-day tropical oscillation — a review. *Mon Wea Rev* 122:814–837. https://doi.org/10.1175/1520-0493(1994)122<0814:OOTDTO>2.0.CO;2
- Mapes BE (2000). Convective inhibition, subgrid-scale triggering energy, and stratiform instability in a toy tropical wave model. *J Atmos Sci* 57:1515–1535. https://doi.org/10.1175/1520-0469(2000)057<1515:CISSTE>2.0.CO;2
- Mason SJ, Graham NE (2002). Areas beneath the relative operating characteristics (ROC) and relative operating levels (ROL) curves: statistical significance and interpretation. *Q J R Meteorol Soc* 128:2145–2166. https://doi.org/10.1256/003590002320603584
- Matthews AJ (2000). Propagation mechanisms for the Madden-Julian Oscillation. *Q J R Meteorol Soc* 126:2637–2651. https://doi.org/10.1002/qj.49712656902
- McBride JL, Nicholls N (1983). Seasonal relationships between Australian rainfall and the Southern Oscillation. *Mon Wea Rev* 111:1998–2004. https://doi.org/10.1175/1520-0493(1983)111<1998:SRBARA>2.0.CO;2
- Meyers G, McIntosh P, Pigot L, Pook M (2007). The years of El Niño, La Niña, and interactions with the tropical Indian Ocean. *J Clim* 20:2872–2880. https://doi.org/10.1175/JCLI4152.1
- Murphy AH (1988). Skill scores based on the mean square error and their relationships to the correlation coefficient. *Mon Wea Rev* 116:2417–2424. https://doi.org/10.1175/1520-0493(1988)116<2417:SSBOTM>2.0.CO;2

- Neelin JD, Peters O, Hales K (2009). The transition to strong convection. *J Atmos Sci* 66:2367–2384. https://doi.org/10.1175/2009JAS2962.1
- Nicholson SE (2017). Climate and climatic variability of rainfall over eastern Africa. *Rev Geophys* 55:590–635. https://doi.org/10.1002/2016RG000544
- Peatman SC, Matthews AJ, Stevens DP (2014). Propagation of the Madden–Julian Oscillation through the Maritime Continent and scale interaction with the diurnal cycle of precipitation. *Q J R Meteorol Soc* 140:814–825. https://doi.org/10.1002/qj.2161
- Pepe MS (2003). *The Statistical Evaluation of Medical Tests for Classification and Prediction.* Oxford University Press, Oxford.
- Pohl B, Camberlin P (2006). Influence of the Madden–Julian Oscillation on East African rainfall. I: Intraseasonal variability and regional dependency. *Q J R Meteorol Soc* 132:2521–2539. https://doi.org/10.1256/qj.05.104
- Pohl B, Matthews AJP (2007). Observed changes in the lifetime and amplitude of the Madden–Julian Oscillation associated with interannual ENSO sea surface temperature anomalies. *J Clim* 20:2659–2674. https://doi.org/10.1175/JCLI4230.1
- Qian JH (2008). Why precipitation is mostly concentrated over islands in the Maritime Continent. *J Atmos Sci* 65:1428–1441. https://doi.org/10.1175/2007JAS2422.1
- Ramage CS (1968). Role of a tropical "Maritime Continent" in the atmospheric circulation. *Mon Wea Rev* 96:365–370. https://doi.org/10.1175/1520-0493(1968)096<0365:ROATMC>2.0.CO;2
- Rasmusson EM, Carpenter TH (1982). Variations in tropical sea surface temperature and surface wind fields associated with the Southern Oscillation/El Niño. *Mon Wea Rev* 110:354–384. https://doi.org/10.1175/1520-0493(1982)110<0354:VITSST>2.0.CO;2
- Raymond DJ, Herman MJ (2011). Convective quasi-equilibrium reconsidered. *J Adv Model Earth Syst* 3:M08003. https://doi.org/10.1029/2011MS000079
- Reason CJC, Rouault M (2002). ENSO-like decadal variability and South African rainfall. *Geophys Res Lett* 29:1638. https://doi.org/10.1029/2002GL014663
- Reichle RH, Liu Q, Koster RD, et al (2017). Land surface precipitation in MERRA-2. *J Clim* 30:1643–1664. https://doi.org/10.1175/JCLI-D-16-0570.1
- Ropelewski CF, Halpert MS (1987). Global and regional scale precipitation patterns associated with the El Niño/Southern Oscillation. *Mon Wea Rev* 115:1606–1626. https://doi.org/10.1175/1520-0493(1987)115<1606:GARSPP>2.0.CO;2
- Roundy PE (2012). The spectrum of convectively coupled Kelvin waves and the Madden–Julian Oscillation in regions of low-level easterly and westerly background flow. *J Atmos Sci* 69:2107–2111. https://doi.org/10.1175/JAS-D-12-060.1
- Rui H, Wang B (1990). Development characteristics and dynamic structure of tropical intraseasonal convection anomalies. *J Atmos Sci* 47:357–379. https://doi.org/10.1175/1520-0469(1990)047<0357:DCADSO>2.0.CO;2
- Saji NH, Goswami BN, Vinayachandran PN, Yamagata T (1999). A dipole mode in the tropical Indian Ocean. *Nature* 401:360–363. https://doi.org/10.1038/43848

- Saji NH, Yamagata T (2003). Possible impacts of Indian Ocean Dipole mode events on global climate. *Clim Res* 25:151–169. https://doi.org/10.3354/cr025151
- Shenigarapu P, Ekkaluri SR (2026). MJO phase-response diagnostic skill reflects convective regime contingency beyond coupling strength across tropical sites. EarthArXiv [Preprint].https://doi.org/12276
- Stackhouse PW Jr, Zhang T, Westberg D, Barnett AJ, Bristow T, Macpherson B, Hoell JM (2018). *POWER release 8 (with GIS applications) methodology (data parameters, sources, and validation). NASA Technical Report, Version 8.0.1.* NASA Langley Research Centre, Hampton.
- Straub KH (2013). MJO initiation in the real-time multivariate MJO index. *J Clim* 26:1130–1151. https://doi.org/10.1175/JCLI-D-12-00074.1
- Suematsu T, Martin ZK, Barnes EA, DeMott CA, Hagos S, Ham YG, Kim D, Kim H, Koh T-Y, Maloney ED (2024). Incorrect computation of Madden-Julian oscillation prediction skill. *npj Clim Atmos Sci* 7:148. https://doi.org/10.1038/s41612-024-00687-1
- Sultan B, Janicot S (2003). The West African monsoon dynamics. Part II: The "preonset" and "onset" of the summer monsoon. *J Clim* 16:3407–3427. https://doi.org/10.1175/1520-0442(2003)016<3407:TWAMDP>2.0.CO;2
- Suppiah R (1997). Extremes of the Southern Oscillation phenomenon and rainfall of Sri Lanka. *Int J Climatol* 17:87–101. https://doi.org/10.1002/(SICI)1097-0088(199701)17:1<87::AID-JOC95>3.0.CO;2-8
- Trenberth KE (1997). The definition of El Niño. *Bull Am Meteorol Soc* 78:2771–2777. https://doi.org/10.1175/1520-0477(1997)078<2771:TDOENO>2.0.CO;2
- Trenberth KE, Branstator GW, Karoly D, Kumar A, Lau N-C, Ropelewski C (1998). Progress during TOGA in understanding and modelling global teleconnections associated with tropical sea surface temperatures. *J Geophys Res* 103:14291–14324. https://doi.org/10.1029/97JC01444
- Vinayachandran PN, Saji NH, Yamagata T (1999). Response of the equatorial Indian Ocean to an unusual wind event during 1994. *Geophys Res Lett* 26:1613–1616. https://doi.org/10.1029/1999GL900272
- Vitart F (2017). Madden–Julian Oscillation prediction and teleconnections in the S2S database. *Q J R Meteorol Soc* 143:2210–2220. https://doi.org/10.1002/qj.3079
- Vitart F, Robertson AW (2018). The sub-seasonal to seasonal prediction project (S2S) and the prediction of extreme events. *npj Clim Atmos Sci* 1:3. https://doi.org/10.1038/s41612-018-0018-0
- Wallace JM, Gutzler DS (1981). Teleconnections in the geopotential height field during the Northern Hemisphere winter. *Mon Wea Rev* 109:784–812. https://doi.org/10.1175/1520-0493(1981)109<0784:TITGHF>2.0.CO;2
- Webster PJ, Moore AM, Loschnigg JP, Leben RR (1999). Coupled ocean–atmosphere dynamics in the Indian Ocean during 1997–98. *Nature* 401:356–360. https://doi.org/10.1038/43848
- Wheeler MC, Hendon HH (2004). An all-season real-time multivariate MJO index: development of an index for monitoring and prediction. *Mon Wea Rev* 132:1917–1932. https://doi.org/10.1175/1520-0493(2004)132<1917:AARMMI>2.0.CO;2

- Wheeler MC, McBride JL (2005). Australian–Maritime Continent rainfall variability. In: Lau W, Waliser D (eds) *Intraseasonal Variability in the Atmosphere–Ocean Climate System.* Praxis, Chichester, pp 125–173.
- Wilks DS (2019). *Statistical Methods in the Atmospheric Sciences,* 4th edn. Elsevier, Amsterdam.
- Zhang C (2005). Madden-Julian Oscillation. *Rev Geophys* 43:RG2003. https://doi.org/10.1029/2004RG000158
- Zscheischler J, Martius O, Westra S, Bevacqua E, Raymond C, Horton RM, van den Hurk B, AghaKouchak A, Jézéquel A, Mahecha MD, Maraun D, Ramos AM, Ridder NN, Thiery W, Vignotto E (2020). A typology of compound weather and climate events. *Nat Rev Earth Environ* 1:333–347. https://doi.org/10.1038/s43017-020-0060-z